A well-balanced approximate Riemann solver for compressible flows in variable cross-section ducts

Philippe Helluy, Jean-Marc Hérard, Hélène Mathis

A well-balanced approximate Riemann solver for compressible flows in variable cross-section ducts

Philippe Helluy

IRMA, Université de Strasbourg,
7 rue Descartes, 67084 Strasbourg, France.
Email : helluy@math.unistra.fr

Jean-Marc Hérard

Corresponding author.
EDF, R&D, Fluid Dynamics, Power Generation and Environment,
6 quai Watier, 78400 Chatou, France.
Phone: (33) 1 30 87 70 37. Fax: (33) 1 30 87 79 16
Email: Jean-Marc.Herard@edf.fr

Hélène Mathis

IRMA, Université de Strasbourg,
7 rue Descartes, 67084 Strasbourg, France.
Email : mathis@math.unistra.fr

Abstract

A well-balanced approximate Riemann solver is introduced in this paper in order to compute approximations of one-dimensional Euler equations in variable cross-section ducts. The interface Riemann solver is grounded on VFRoe-ncv scheme, and it enforces the preservation of Riemann invariants of the steady wave. The main properties of the scheme are detailed. We provide numerical results to assess the validity of the scheme, even when the cross section is discontinuous. A first series is devoted to analytical test cases, and the last results correspond to the simulation of a bubble collapse.

Keywords: Well-balanced scheme, Approximate Riemann solver, Compressible flows, Riemann problem

1. Introduction

For some industrial applications, we need to compute approximations of solutions of partial differential equations (PDE) modelling the flow of a compressible fluid in porous media or in variable cross-section ducts. This may occur while predicting single-phase or two-phase flows. In all cases, some non conservative terms are present in the set of PDE, which correspond to the contribution of pressure effects. In practice, these situations may occur when predicting flows in pipelines or in the primary circuit of a nuclear power plant, or in many other industrial sets. Quite recently, many authors have investigated this subject, both from a theoretical and from a numerical point of view, among which we may quote the papers [2, 4, 5, 11, 13, 15, 17, 18, 19, 21, 22].

In a recent work devoted to two-phase flow modelling ([9, 10]), it has been shown that classical solvers may fail at predicting relevant approximations of this kind of flows, when the cross-section (or alternatively the porosity) becomes discontinuous. This study has been performed while focusing on two-fluid models, but the structure of PDE is such that consequences are the same for single phase or homogeneous two-phase flow models. In particular, it has been proved in [9] that standard solvers may develop rather spurious approximations when restricting to coarse meshes and even more may converge to wrong solutions when the mesh size tends to zero. A way to handle this rather difficult problem is grounded on Greenberg-Leroux [13] and Kröner-Thanh ideas [18]. Actually the very simple solver proposed in [18] enables to recover a correct convergence when investigating solutions of Riemann problems with a discontinuous cross section. However, a drawback of the latter approach is that the accuracy of the resulting scheme is rather poor. Hence, the basic idea that has motivated the present work is to blend both ideas, hence taking advantage of the accuracy of *approximate* Godunov solvers such as those introduced in reference [3], while accounting for the well-balanced spirit of [13, 18, 9, 19, 17], in order to converge towards correct solutions in all situations.

Thus, our main goal in this paper is to detail a new accurate *well-balanced* approximate Riemann solver that enables to perform computations involving both smooth and discontinuous cross sections. The well-known strategy of well-balanced solvers was introduced in [13], and revisited by numerous

authors recently (see [1, 11] among others). A drawback of the well-balanced approach [13] is that the *exact* Godunov interface solver complexifies the code, and meanwhile substantially increases the CPU time. The basic idea is to upwind so-called source terms in a suitable way, in order to maintain all steady solutions on coarse meshes. By the way, we insist that this should not be confused with solvers that only maintain steady solutions involving flows *at rest* (which is actually a subclass of the latter class). The present scheme has been built in such a way that *Riemann invariants of the steady wave are perfectly preserved*, both for interface and cell values, since this seems mandatory in order to guarantee convergence towards relevant solutions when the mesh is refined.

The paper is organised as follows. We first briefly recall the set of governing equations and its main properties. Then we detail the well-balanced approximate Godunov solver, and exhibit its main properties. Eventually, we provide a few results of computations of Riemann problems and then some results in a difficult situation corresponding to the sudden collapse of a spherical bubble.

2. Compressible model

2.1. Governing equations

We consider one-dimensional flows of a compressible fluid that is characterized by its mean density $\rho(x,t)$, its mean pressure $P(x,t)$, and the mean velocity $U(x,t)$ within the cross section.

We define the cross-section $A(x) > 0$ through which the fluid flows. The function $A(x)$ must be given in each case. For some applications, we will use in practice spherical geometries, which means that we will have $A(x) = 4\pi x^2$. We define classically the total energy E:

$$E(x,t) = \rho(x,t)U(x,t)^2/2 + \rho(x,t)e(P(x,t),\rho(x,t))$$

in terms of the internal energy $e(P,\rho)$ which is provided by the equation of state (EOS). The conservative state variable W is noted:

$$W^t = (A, A\rho, A\rho U, AE) \ . \tag{1}$$

The governing equations of the fluid are:

$$\left\{ \begin{array}{l} \partial_t \left(A \right) = 0 \ ; \\ \partial_t \left(A\rho \right) + \partial_x \left(A\rho U \right) = 0 \ ; \\ \partial_t \left(A\rho U \right) + \partial_x \left(A\rho U^2 \right) + A\partial_x \left(P \right) = 0 \ ; \\ \partial_t \left(AE \right) + \partial_x \left(AU(E+P) \right) = 0 \ . \end{array} \right. \tag{2}$$

If we note:

$$\left\{ \begin{array}{l} f^t(W) = (0, A\rho U, A\rho U^2, AU(E+P)) \ , \\ g^t(W) = (0, 0, P, 0) \ , \end{array} \right. \tag{3}$$

System (2) may be rewritten:

$$\partial_t \left(W \right) + \partial_x \left(f(W) \right) + A\partial_x \left(g(W) \right) = 0 \ . \tag{4}$$

We also introduce the specific entropy S that must comply with:

$$\frac{\partial_P \left(S(P,\rho) \right) |_\rho}{\partial_\rho \left(S(P,\rho) \right) |_P} = \frac{-1}{(c)^2(P,\rho)} \ . \tag{5}$$

In the latter equation, the speed of sound waves c is defined by:

$$c(P,\rho) = \left(\frac{\frac{P}{(\rho)^2} - \partial_\rho \left(e(P,\rho) \right) |_P}{\partial_P \left(e(P,\rho) \right) |_\rho} \right)^{1/2} \ . \tag{6}$$

Eventually, we need to introduce two additional intermediate variables:

1. the total enthalpy $H \stackrel{def}{=} e(P,\rho) + \frac{P}{\rho} + \frac{U^2}{2} = h(P,\rho) + \frac{U^2}{2}$, where h denotes the enthalpy,
2. the mean discharge $Q \stackrel{def}{=} A\rho U$.

2.2. Properties

We briefly recall some basic properties below. For that purpose, we introduce the condensed form of (2) which reads:

$$\partial_t \left(W \right) + B(W)\partial_x \left(W \right) = 0 \ . \tag{7}$$

Property 1 (*Hyperbolicity and entropy inequality*)
System (2) *has four real eigenvalues:*

$$\lambda_0 = 0 \quad ; \quad \lambda_1 = U \quad ; \quad \lambda_2 = U - c \quad ; \quad \lambda_3 = U + c \tag{8}$$

The set of right eigenvectors of $B(W)$ spans the whole space if $|U| \neq c$. The $0, 1$ fields are linearly degenerated. Other fields are genuinely non linear. Moreover, if we note:

$$\eta = A\rho Log(S) \quad ; \quad f_\eta = A\rho Log(S)U$$

the entropy-entropy flux pair, smooth solutions $W(x,t)$ of (2) agree with:

$$\partial_t(\eta) + \nabla.(f_\eta) = 0 \ . \tag{9}$$

This result is classical. One may for instance use the variable $Y = (A, S, \rho, U)$ is useful to check that property. When $U^2 - c^2 = \lambda_2\lambda_3 = 0$, the set of right eigenvectors spans $\mathbf{R}^3$. On the other hand, this set spans $\mathbf{R}^4$ when $\lambda_1 = U = 0$, which corresponds to a superposition of two linearly degenerate fields.

We now detail the structure of the two Linearly Degenerate (LD) waves associated with λ_0 and λ_1. A straightforward computation provides the following result:

Property 2 (*Riemann invariants in the LD waves*)
Riemann invariants of the LD steady wave associated with λ_0 are:

$$I_1^0(W) = S \quad ; \quad I_2^0(W) = Q \quad ; \quad I_3^0(W) = H \ .$$

Riemann invariants of the LD wave associated with λ_1 are:

$$I_1^1(W) = A \quad ; \quad I_2^1(W) = U \quad ; \quad I_3^1(W) = P \ .$$

The structure of the LD wave associated with λ_0 will be the keystone of the well-balanced scheme. We may now present the Finite Volume procedure.

3. A well-balanced Finite Volume scheme for compressible flows in variable cross-section ducts

3.1. Computing cell values

We introduce now a rather simple well-balanced Finite Volume scheme. We recall first that the basic ideas of well-balanced schemes have been introduced by Greenberg and Leroux in the early paper [13]. The concept has been used extensively (see [8, 1, 15] for instance, among others). In order to

present the scheme, we first need to define W_i^n which is an approximation of the mean value of W at time t^n within each Finite Volume Ω_i of size h_i

$$W_i^n \simeq \frac{1}{h_i} \int_{\Omega_i} W(x, t^n) dx \ . \tag{10}$$

Moreover, we define:

$$\overline{a}_{i+1/2} = (a_i + a_{i+1})/2 \quad ; \quad \Delta a_{i+1/2} = (a_{i+1} - a_i) \quad ; \quad \delta a_i = (a_i^{n+1} - a_i^n).$$

We may now introduce the new variable

$$Z^t = (A, S, Q, H)$$

in $\mathbf{R}^4$. The discrete variable A_i is assumed to be constant within each cell i. The computation of the scheme is performed by the following update:

$$\begin{aligned} h_i(W_i^{n+1} - W_i^n) + \Delta t^n \left(F_{i+1/2,-}(Z_i^n, Z_{i+1}^n) - F_{i-1/2,+}(Z_{i-1}^n, Z_i^n) \right) \\ + \Delta t^n A_i \left(G_{i+1/2,-}(Z_i^n, Z_{i+1}^n) - G_{i-1/2,+}(Z_{i-1}^n, Z_i^n) \right) = 0. \end{aligned} \tag{11}$$

The time step Δt^n must comply with a CFL condition. The numerical flux $F_{i+1/2,-}$ is defined by:

$$F_{i+1/2,-}(Z_i^n, Z_{i+1}^n) \stackrel{def}{=} f(W(Z_{i+1/2,-})), \tag{12}$$

and the pressure contribution is similar:

$$G_{i+1/2,-}(Z_i^n, Z_{i+1}^n) \stackrel{def}{=} g(W(Z_{i+1/2,-})). \tag{13}$$

We must now detail how to compute interface values $Z_{i+1/2,\pm}$, and also how to get back to W.

3.2. Computing interface values $Z_{i+1/2,\pm}$

In order to define interface states $Z_{i+1/2,-}$ and $Z_{i-1/2,+}$ we proceed as follows. For regular solutions, system (2) may be rewritten in the form:

$$\left\{ \begin{array}{l} \partial_t (A) = 0 \ ; \\ \partial_t (S) + U \partial_x (S) = 0 \ ; \\ \partial_t (Q) + U \partial_x (Q) + \rho A \partial_x (H) + A(\partial_S (P) \mid_\rho - \rho \partial_S (h) \mid_\rho) \partial_x (S) = 0 \ ; \\ \partial_t (H) + U \partial_x (H) + \frac{c^2}{\rho A} \partial_x (Q) + \frac{U}{\rho} \partial_S (P) \mid_\rho \partial_x (S) = 0 \ , \end{array} \right. \tag{14}$$

or in a condensed form as:

$$\partial_t (Z) + C(Z)\partial_x (Z) = 0 \ . \tag{15}$$

We define the right eigenvectors $r_k(Z)$ of $C(Z)$:

$$\left\{ \begin{array}{l} r_0(Z) = (1, 0, 0, 0) \\ r_1(Z) = (0, 1, -\frac{Au}{c^2}\partial_S (P) \, , b(\rho, S)) \\ r_2(Z) = (0, 0, \rho A, -c) \\ r_3(Z) = (0, 0, \rho A, c) \end{array} \right. \tag{16}$$

setting $b(\rho, S) = -\frac{1}{\rho}(\partial_S (P) \mid_\rho - \rho \partial_S (h) \mid_\rho$.

Before going further on, we note that *this set of right eigenvectors always spans* $\mathbf{R}^4$*, even when the product* $\lambda_2 \lambda_3$ *vanishes (unless a vacuum occurs in the solution).* This is easy to check: if we define Ω the matrix of right eigenvectors (r_0, r_1, r_2, r_3), the determinant reads: $det(\Omega) = 2\rho A c$.

Now, rather than computing interface states $Z_{i+1/2,-}$ and $Z_{i+1/2,+}$ by solving the exact Riemann problem associated with (14), these states are computed by solving a linear Riemann problem associated with the following system:

$$\partial_t (Z) + C(\hat{A}, \hat{\rho}, \hat{U}, \hat{P})\partial_x (Z) = 0 \tag{17}$$

with given initial condition $Z((x - x_{i+1/2}) < 0, t = 0) = Z_i^n$ and $Z((x - x_{i+1/2}) > 0, t = 0) = Z_{i+1}^n$, and setting the average $\hat{\phi}$ of any quantity ϕ as:

$$(\hat{\phi})_{i+1/2} = (\beta_\phi)_{i+1/2}\phi_i + (1 - (\beta_\phi)_{i+1/2})\phi_{i+1}.$$

where the β_ϕ coefficient lies in $[0, 1]$. In practice, this coefficient is usually set to $1/2$ in almost all cases (see [3, 7]). Nonetheless, one may also use other averages (see [15] where the harmonic average is used).

For *conservative* systems, VFRoe-ncv scheme is an approximate Godunov scheme, where the intermediate states at the interface $x/t = 0$, that are computed with help of (17), are directly used to evaluate the numerical interface flux function ; thus it is a *conservative* scheme in the conservative framework. As emphasized in [3, 7], the convergence towards the correct shock solutions has been checked extensively by investigating approximate solutions obtained

while computing various Riemann problems involving contact discontinuities, shocks and rarefaction waves, for different systems. The asymptotic rate of convergence in L^1 norm is 1/2 for so-called first order schemes (respectively 2/3 for "second-order" schemes). More precisely, when restricting to first order schemes, pure contact waves converge as $h^{1/2}$, and pure shocks or rarefaction waves converge as h, if h denotes the mean mesh size. The VFRoe-ncv scheme actually requires an entropy correction at sonic points in rarefaction waves, as occurs for many approximate Riemann solvers.

Since our system (2) has no conservative form, the numerical flux will be discontinuous and we need to define our scheme precisely (see below). Owing to the steady contact discontinuity, the solution of the linearized system (17) is discontinuous through the interface $(x - x_{i+1/2})/t = 0$. If we denote $Z^{Riemann}(x/t)$ the solution of the linear Riemann problem associated with (17), we define:

$$Z_{i+1/2,-} = Z^{Riemann}((x - x_{i+1/2})/t = 0^-) \ ,$$

and:

$$Z_{i+1/2,+} = Z^{Riemann}((x - x_{i+1/2})/t = 0^+) \ .$$

In order to detail the construction of the solution of the linearized Riemann problem (17), we introduce the right eigenvectors of the matrix $C(\hat{A}, \hat{\rho}, \hat{U}, \hat{P})$ which are noted:

$$\left\{ \begin{array}{l} \hat{r}_0 = (1, 0, 0, 0) \\ \hat{r}_1 = (0, 1, -\frac{\hat{A}\hat{u}}{c(\hat{P},\hat{\rho})^2}(\partial_S(P))(\hat{P}, \hat{\rho}), b(\hat{\rho}, S(\hat{P}, \hat{\rho}))) \\ \hat{r}_2 = (0, 0, \hat{\rho}\hat{A}, -c(\hat{P}, \hat{\rho})) \\ \hat{r}_3 = (0, 0, \hat{\rho}\hat{A}, c(\hat{P}, \hat{\rho})) \end{array} \right. \tag{18}$$

and the numerical eigenvalues:

$$\left\{ \begin{array}{l} \hat{\lambda}_0 = 0 \\ \hat{\lambda}_1 = \hat{u} \\ \hat{\lambda}_2 = \hat{u} - c(\hat{P}, \hat{\rho}) \\ \hat{\lambda}_3 = \hat{u} + c(\hat{P}, \hat{\rho}) \end{array} \right. \tag{19}$$

The matrix $\hat{\Omega}$ of right eigenvectors $(\hat{r}_0, \hat{r}_1, \hat{r}_2, \hat{r}_3)$ is not singular (see above), and we may decompose $Z_R - Z_L$ as follows:

$$Z_{i+1} - Z_i = \sum_{k=0}^{3} \alpha_k \hat{r}_k$$

and compute:

$$(\alpha_0, \alpha_1, \alpha_2, \alpha_3)^t = (\hat{\Omega})^{-1}(Z_{i+1} - Z_i)$$

which read:

$$\left\{ \begin{array}{l} \alpha_0 = A_{i+1} - A_i \\ \alpha_1 = S_{i+1} - S_i \\ \alpha_2 = \gamma(S_{i+1} - S_i) + (Q_{i+1} - Q_i)/(2\hat{\rho}\hat{A}) - (H_{i+1} - H_i)/(2c(\hat{P}, \hat{\rho})) \\ \alpha_3 = \delta(S_{i+1} - S_i) + (Q_{i+1} - Q_i)/(2\hat{\rho}\hat{A}) + (H_{i+1} - H_i)/(2c(\hat{P}, \hat{\rho})) \end{array} \right. \tag{20}$$

where: $\gamma + \delta = \hat{U}/(\hat{\rho}(c(\hat{P}, \hat{\rho})^2)$, and: $-\gamma + \delta = -b(\hat{\rho}, S(\hat{P}, \hat{\rho}))/c(\hat{P}, \hat{\rho})$.

Obviously, we note that if:

$$S_{i+1} - S_i = Q_{i+1} - Q_i = H_{i+1} - H_i = 0 \ ,$$

we get in a straightforward way: $\alpha_1 = \alpha_2 = \alpha_3 = 0$. Thus in that particular case, we get:

$$Z((x - x_{i+1/2})/t < 0) = Z_{i+1} \quad \textit{and :} \quad Z((x - x_{i+1/2})/t > 0) = Z_i$$

whatever A_i and A_{i+1} are. This will be one important ingredient in the proof of Proposition 2.

We may now detail all interface states that are then defined by:

- If $\hat{\lambda}_2 > 0$, then $Z_{i+1/2,-} = Z_i$ and $Z_{i+1/2,+} = Z_i + \alpha_0 \hat{r}_0$;
- If $\hat{\lambda}_2 < 0$ and $\hat{\lambda}_1 > 0$, then $Z_{i+1/2,-} = Z_i + \alpha_2 \hat{r}_2$ and $Z_{i+1/2,+} = Z_i + \alpha_2 \hat{r}_2 + \alpha_0 \hat{r}_0$;
- If $\hat{\lambda}_1 < 0$ and $\hat{\lambda}_3 > 0$, then $Z_{i+1/2,-} = Z_{i+1} - \alpha_3 \hat{r}_3 - \alpha_0 \hat{r}_0$ and $Z_{i+1/2,+} = Z_{i+1} - \alpha_3 \hat{r}_3$;
- If $\hat{\lambda}_3 < 0$, then $Z_{i+1/2,-} = Z_{i+1} - \alpha_0 \hat{r}_0$ and $Z_{i+1/2,+} = Z_{i+1}$.

Thus, we get: $Z_{i+1/2,+} - Z_{i+1/2,-} = \alpha_0 \hat{r}_0$. Moreover, in specific situations where eigenvalues vanish, we define in a natural way:

- If $\hat{\lambda}_1 = 0$, then $Z_{i+1/2,-} = Z_i + \alpha_2 \hat{r}_2$ and $Z_{i+1/2,+} = Z_{i+1} - \alpha_3 \hat{r}_3$;
- If $\hat{\lambda}_2 = 0$, then $Z_{i+1/2,-} = Z_i$ and $Z_{i+1/2,+} = Z_{i+1} - \alpha_3 \hat{r}_3 - \alpha_1 \hat{r}_1$;

- If $\hat{\lambda}_3 = 0$, then $Z_{i+1/2,-} = Z_i + \alpha_2 \hat{r}_2 + \alpha_1 \hat{r}_1$ and $Z_{i+1/2,+} = Z_{i+1}$.

We now provide a first result which is the following:

Proposition 1: (*Well-balanced interface solver*)
We assume that $\hat{\lambda}_1 \hat{\lambda}_2 \hat{\lambda}_3 \neq 0$. *Then, the interface Riemann solver computes intermediate states which are such that:*

$$Q_{i+1/2,-} = Q_{i+1/2,+} \quad ; \quad H_{i+1/2,-} = H_{i+1/2,+} \quad ; \quad S_{i+1/2,-} = S_{i+1/2,+} \ .$$

Moreover the interface Riemann solver is such that:

$$A_{i+1/2,-} = A_i \quad \text{and:} \quad A_{i-1/2,+} = A_i \ .$$

Proof:
The proof is obvious : if $\hat{\lambda}_1 \hat{\lambda}_2 \hat{\lambda}_3 \neq 0$, owing to the form of the first right eigenvector $\hat{r}_0$ (see (18)), we get:

$$Z_{i+1/2,+} - Z_{i+1/2,-} = (A_{i+1} - A_i)\hat{r}_0 \ .$$

and thus :

$$[Q]_{i+1/2,-}^{i+1/2,+} = 0 \quad ; \quad [H]_{i+1/2,-}^{i+1/2,+} = 0 \quad ; \quad [S]_{i+1/2,-}^{i+1/2,+} = 0 \ ,$$

(where $[\phi]_a^b$ denotes the jump $\phi_b - \phi_a$) but also:

$$A_{i+1/2,+} - A_{i+1/2,-} = A_{i+1} - A_i \ .$$

Moreover, we get $Z_{i+1/2,+} - Z_{i+1/2,-} = \alpha_0 \hat{r}_0 + \alpha_1 \hat{r}_1$ when $\hat{\lambda}_1 = 0$. In that case we have: $[Q]_{i+1/2,-}^{i+1/2,+} = 0$.

Since $A_{i-1/2,+} = A_{i+1/2,-} = A_i$, the scheme (11) may be rewritten in a slightly different form by gettting rid of A_i in all cell equations:

$$h_i(Y_i^{n+1} - Y_i^n) + \quad \Delta t^n \left(L_{i+1/2,-}(Z_i^n, Z_{i+1}^n) - L_{i-1/2,+}(Z_{i-1}^n, Z_i^n) \right) = 0 \ , \tag{21}$$

where:

$$\left\{ \begin{array}{l} Y^t = (A, \rho, \rho U, E) \ , \\ l^t(Y) = (0, \rho U, \rho U^2 + P, U(E+P)) \ , \end{array} \right. \tag{22}$$

and:

$$\left\{ \begin{array}{l} L_{i+1/2,-}(Z_i^n, Z_{i+1}^n) \stackrel{def}{=} l(Y(Z_{i+1/2,-})) \ , \\ L_{i-1/2,+}(Z_{i-1}^n, Z_i^n) \stackrel{def}{=} l(Y(Z_{i-1/2,+})) \ . \end{array} \right. \tag{23}$$

We must now provide definitions of both values $Y(Z_{i+1/2,-})$ and $Y(Z_{i+1/2,+})$ at each cell interface $i + 1/2$.

3.3. Computing interface solutions $\rho_{i+1/2,-}$ and $\rho_{i+1/2,+}$

Once $Z_{i+1/2,-}$ and $Z_{i+1/2,+}$ have been computed, we need to calculate $Y(Z_{i+1/2,-})$ and $Y(Z_{i+1/2,+})$. For that purpose, we will in fact calculate the two densities $\rho_{i+1/2,-}$ and $\rho_{i+1/2,+}$ at each cell interface. This is achieved as follows.

We do not consider any specific form of the equation of state $e(P, \rho)$. Nonetheless, rewriting P in terms of ρ, S, and introducing

$$h(\rho, S) = e(P(\rho, S), \rho) + P(\rho, S)/\rho \ ,$$

we will assume that the following holds:

$$h(0, S) = 0 \quad \text{and:} \quad \lim_{X->+\infty} h(X, S) = +\infty \ , \tag{24}$$

$$\partial_X \left(h(X, S) \right) |_S > 0 \quad \text{and:} \quad \partial_{X^2} \left(h(X, S) \right) |_S > 0 \ , \tag{25}$$

whatever S is.

We now aim at computing the solutions $X^- = \rho^-_{i+1/2}$ and $X^+ = \rho^+_{i+1/2}$ of the equations:

$$j_{i+1/2,-}(X^-) \stackrel{def}{=} (h + U^2/2)(A_i, S^-_{i+1/2}, Q^-_{i+1/2}, X^-) = H^-_{i+1/2} \ , \tag{26}$$

and:

$$j_{i+1/2,+}(X^+) \stackrel{def}{=} (h + U^2/2)(A_{i+1}, S^+_{i+1/2}, Q^+_{i+1/2}, X^+) = H^+_{i+1/2} \ , \tag{27}$$

taking into account the fact that:

$$U_{i+1/2,-} = Q^-_{i+1/2}/(A_i X^-) \quad \text{and:} \quad U_{i+1/2,+} = Q^+_{i+1/2}/(A_{i+1} X^+) \ , \tag{28}$$

and also:

$$h_{i+1/2,-} = h(X^-, S^-_{i+1/2}) \quad \text{and:} \quad h_{i+1/2,+} = h(X^+, S^+_{i+1/2}) \ . \tag{29}$$

- *We focus first on the calculation of X^-.*
  Thus, we study the function:

$$j_{i+1/2,-}(X) = \frac{(Q^-_{i+1/2})^2}{2A_i^2(X)^2} + h(X, S^-_{i+1/2}) \ ,$$

  whose derivatives are:

$$j'_{i+1/2,-}(X) = -\frac{(Q^-_{i+1/2})^2}{A_i^2(X)^3} + \partial_X\left(h\right)|_S(X, S^-_{i+1/2}) \ ,$$

$$j''_{i+1/2,-}(X) = 3\frac{(Q^-_{i+1/2})^2}{A_i^2(X)^4} + \partial_{X^2}\left(h\right)|_S(X, S^-_{i+1/2}) \ .$$

  – If $Q_{i+1/2} = 0$, the equation (26) obviously admits a unique *positive* solution X^- such that:

$$h(X^-, S^-_{i+1/2}) = H^-_{i+1/2} \ .$$

  – Otherwise, we define $X_{min} > 0$ the solution of:

$$X^3_{min}\partial_X\left(h\right)|_S(X_{min}, S^-_{i+1/2}) = (Q^-_{i+1/2})^2/A_i^2 \ .$$

    Owing to the previous assumptions (24), (25) on the equation of state, the function $j_{i+1/2,-}(X)$ is decreasing when $X \in]0, X_{min}]$ and increasing when $X \in [X_{min}, +\infty[$; moreover:

$$\lim_{0^+} j_{i+1/2,-}(X) = +\infty \quad \text{and:} \quad \lim_{+\infty} j_{i+1/2,-}(X) = +\infty \qquad (30)$$

    Thus, two cases may arise:

    * If $j_{i+1/2,-}(X_{min}) < H^-_{i+1/2}$, then, the equation (26) admits two distinct solutions. Using a continuity argument, the solution X^- that is retained is:

$$X^- \in \ ]0, X_{min}] \quad \textit{if:} \quad \rho_i^n \in \ ]0, X_{min}] \qquad (31)$$

      (respectively $X^- \in [X_{min}, +\infty[$ if $\rho_i^n \in [X_{min}, +\infty[$). Hence the solution X^- is in the subsonic (respectively supersonic) branch if the ith cell state is subsonic (respectively supersonic).

* If $H^-_{i+1/2} \leq j_{i+1/2,-}(X_{min})$, the value which is retained is the one that minimizes the quantity $(j_{i+1/2,-}(X) - H^-_{i+1/2})^2$, that is: $X^- = X_{min}$.

Numerical fluxes $f(W(Z_{i+1/2,-}))$ and $g(W(Z_{i+1/2,-}))$ are now uniquely defined.

- *We now turn to the computation of X^+.*
  We compute now in the same manner $X^+ = \rho_{i+1/2,+}$, studying the function:

$$j_{i+1/2,+}(X) - H^+_{i+1/2} = \frac{(Q^+_{i+1/2})^2}{2A^2_{i+1}(X)^2} + h(X, S^+_{i+1/2}) - H^+_{i+1/2} \ .$$

  We are now in cell $i+1$, and thus the reference is ρ^n_{i+1} when two solutions arise. This means that the solution is $X^+ \in]0, X_{Min}]$ if $\rho^n_{i+1} \in]0, X_{Min}]$ (respectively $X^+ \in [X_{Min}, +\infty[$ if $\rho^n_{i+1} \in [X_{Min}, +\infty[$) where $X_{Min} > 0$ is the solution of:

$$X^3_{Min} \partial_X (h) \mid_S (X_{Min}, S^+_{i+1/2}) = (Q^+_{i+1/2})^2 / A^2_{i+1} \ .$$

The definition of the scheme (11), (12), (13) is now complete.

3.4. Remarks

Remark 1- The particular case of a perfect gas EOS

We only detail here the case where the equation of state of the fluid follows a perfect gas law, that is:

$$e(P, \rho) = P/((\gamma - 1)\rho).$$

In that particular case, we get $S = P/\rho^\gamma$ and thus:

$$j_{i+1/2,-}(X) = \gamma/(\gamma - 1) S^-_{i+1/2} X^{\gamma - 1} + (Q^-_{i+1/2})^2/(2A^2_i X^2) \ ,$$

$$j_{i+1/2,+}(X) = \gamma/(\gamma - 1) S^+_{i+1/2} X^{\gamma - 1} + (Q^+_{i+1/2})^2/(2A^2_{i+1} X^2) \ .$$

The function $j_{i+1/2,-}(X)$ (respectively $j_{i+1/2,+}(X)$) is decreasing when X lies in $[0, X_{min}]$ (respectively in $[0, X_{Min}]$), and increasing in $[X_{min}, +\infty[$ (respectively in $[X_{Min}, +\infty[$), while setting:

$$X_{min} = (Q^2_{i+1/2}/(\gamma A^2_i S_{i+1/2}))^{1/(\gamma+1)} \quad ; \quad X_{Min} = (Q^2_{i+1/2}/(\gamma A^2_{i+1} S_{i+1/2}))^{1/(\gamma+1)} \ .$$

Remark 2- Entropy correction at sonic points in rarefaction waves
An entropy fix is required at sonic points in rarefaction waves for the present approximate Riemann solver. We use here a very simple and efficient parameter-free entropy correction that has been introduced in [14].

4. Main property of the scheme

This scheme preserves flows at rest, even when the cross-section A is not uniform. Actually, we have:

Proposition 2: (*Well-balanced scheme*)
We consider arbitrary values of A_i, and initial data such that for all i:

$$S_i = S_0 \quad ; \quad Q_i = Q_0 \quad ; \quad H_i = H_0 \ .$$

Then the scheme (11) *introduced above preserves steady states on any mesh, i.e.:*

$$\delta\rho_i = 0 \quad ; \quad \delta U_i = 0 \quad ; \quad \delta E_i = 0 \ .$$

Thus the scheme is well-balanced.

Proof:
The proof is obtained by construction.

- We start with the mass balance equation:

$$h_i(\rho_i^{n+1} - \rho_i^n) + \Delta t^n \left(\rho_{i+1/2,-} U_{i+1/2,-} - \rho_{i-1/2,+} U_{i-1/2,+}\right) = 0 \ .$$

  The initial conditions and the interface solver guarantee that:

$$Q_i^n = Q_{i+1}^n = Q_0 \quad \text{and:} \quad A_{i+1/2,-}\rho_{i+1/2,-}U_{i+1/2,-} = Q_0 \ ,$$

  but also:

$$Q_i^n = Q_{i-1}^n = Q_0 \quad \text{and:} \quad A_{i-1/2,+}\rho_{i-1/2,+}U_{i-1/2,+} = Q_0 \ .$$

  Owing to the fact that: $A_{i+1/2,-} = A_{i-1/2,+} = A_i$, we deduce: $\rho_{i+1/2,-}U_{i+1/2,-} = \rho_{i-1/2,+}U_{i-1/2,+}$. Hence: $\delta\rho_i = 0$.

- We turn then to the momentum discrete equation. The initial condition and the approximate interface solver will provide interface quantities so that:

$$H_0 = h(S_0, \rho^n_{i+1}) + (U^n_{i+1})^2/2 = h(S_0, \rho_{i+1/2,-}) + (U_{i+1/2,-})^2/2 \ ,$$

and:

$$H_0 = h(S_0, \rho^n_{i-1}) + (U^n_{i-1})^2/2 = h(S_0, \rho_{i-1/2,+}) + (U_{i-1/2,+})^2/2 \ .$$

Hence, taking the previous identity $\rho_{i+1/2,-}U_{i+1/2,-} = \rho_{i-1/2,+}U_{i-1/2,+} = q_0$ into account, we get:

$$\rho_{i-1/2,+} = \rho_{i+1/2,-} \quad \text{and:} \quad U_{i-1/2,+} = U_{i+1/2,-} \ ,$$

owing to the choice of the solution that depends on the cell value (see (31)*).* As a consequence, we also get:

$$P_{i+1/2,-} = P(\rho_{i+1/2,-}, S_0) = P(\rho_{i-1/2,+}, S_0) = P_{i-1/2,+} \ .$$

This eventually results in: $\delta(\rho_i U_i) = 0$, and hence: $\delta U_i = 0$, since we now know that $\delta\rho_i = 0$.

- Using similar arguments, we may complete the proof for the total energy discrete equation, and get $\delta E_i = 0$, since: $(U(E+P))_{i-1/2,+} = (U(E+P))_{i+1/2,-}$.

We emphasize that Proposition 2 is not only useful for practical computations, but that it also seems mandatory in order to ensure convergence towards the relevant solution when the section is not smooth (see [9, 10]).

5. Numerical results

We restrict to unsteady cases, except in the first Riemann problem, which aims at illustrating the well-balanced property proved in Proposition 2. The interface solver used herein relies on the arithmetic average for (ρ, U, P) and on the harmonic average for A.

In a first series, we focus on the computation of four distinct Riemann problems, with *discontinuous values of the cross section*. The first one corresponds to a steady contact discontinuity. The second one involves two contact discontinuities only. The third one, which contains two contact discontinuities together with a one-rarefaction wave and a 3-shock wave, is taken from [21]. Two shock waves and two contact waves arise in the fourth Riemann problem. Exact Riemann solutions can be found using reference [24] for instance.

Next we turn to a very difficult test case that has been inspired by [20]. In this case which mimics the collapse of a bubble, *the cross section is smooth*. The initial ratio of pressures and densities on each side of the initial discontinuity are actually close to 10^5.

In all cases, computations have been performed using a time step in agreement with the CFL condition $CFL = 1/2$.

5.1. Preservation of non-trivial steady states

This test case is aimed at illustrating Proposition 2. Thus we consider an initial data where the left and right states are chosen in order to guarantee a steady solution. We wish to check whether the discrete cell values will remain unchanged when $t > 0$. Initial data are given below:

	Left state	Right state
A	1.	1.1
ρ	1.	1.1314126
U	1.	0.8035007
P	1.	1.1886922

We use a perfect gas state law:

$$P = (\gamma - 1)(E - \rho U^2/2) \ , \tag{32}$$

setting: $\gamma = 7/5$, and the initial discontinuity of the Riemann problem is located at $x = 0.4$. *We note that left and right velocities are non zero values.* The right state given above has been obtained by prescribing $A_R = 1.1$, and then enforcing Riemann invariants of the steady wave -defined in property 2- to be uniform: $I_k^0(W_R) = I_k^0(W_L)$.

We consider a regular mesh with one thousand cells. We compute approximations of the solution over 1000 time iterations, and we plot numerical results for the density. We check here that the well-balanced scheme perfectly preserves the initial data, looking at Figure 1. This of course is in agreement with the statement in Proposition 2.

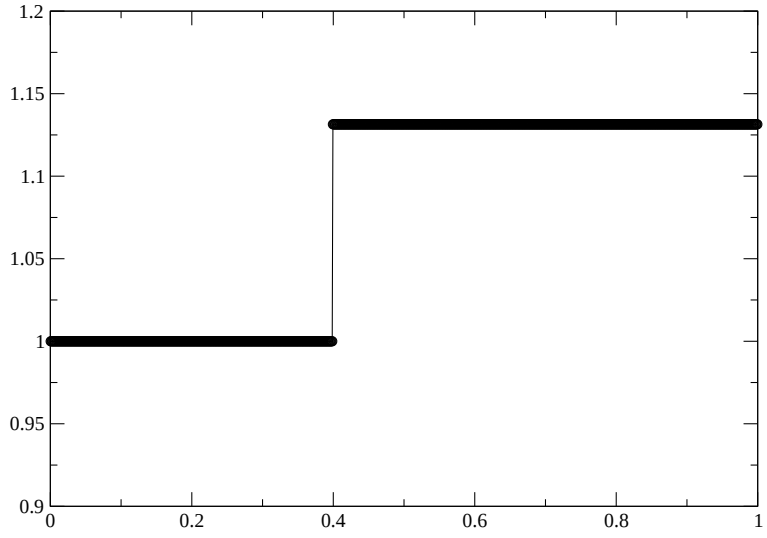

Figure 1: Steady test case: mean density profile.

5.2. Three distinct Riemann problems

5.2.1. A Riemann problem involving two contact discontinuities

We turn now to a slightly different case involving the steady contact discontinuity and a moving contact discontinuity. This case is equivalent to one of those introduced in [9]. The equation of state is still the same as before ((32) with $\gamma = 7/5$). The initial conditions are now the following:

	Left state	State A	Right state
A	1.	2.	2.
ρ	1.	1.3359863	1.
U	1.	0.3742553	0.3742553
P	1.	1.5001089	1.5001089

Thus the -sole- intermediate state between the two contact discontinuities $x/t = 0$ and $x/t = U_1$ is such that: $(U_1, P_1) = (U_R, P_R)$ and $\rho_1 = 1.3359863$. Figures 2 and 3 show the density, pressure, velocity and entropy profiles, focusing on two regular meshes with 100 and 20000 cells respectively. Once again, the steady contact discontinuity is not smeared at all, in agreement with the previous test cases. The smearing of the moving contact discontinuity is classical. Owing to the structure of the solution, it may be checked that the convergence rate is very close to 1/2 in L^1 norm (see Figure 4).

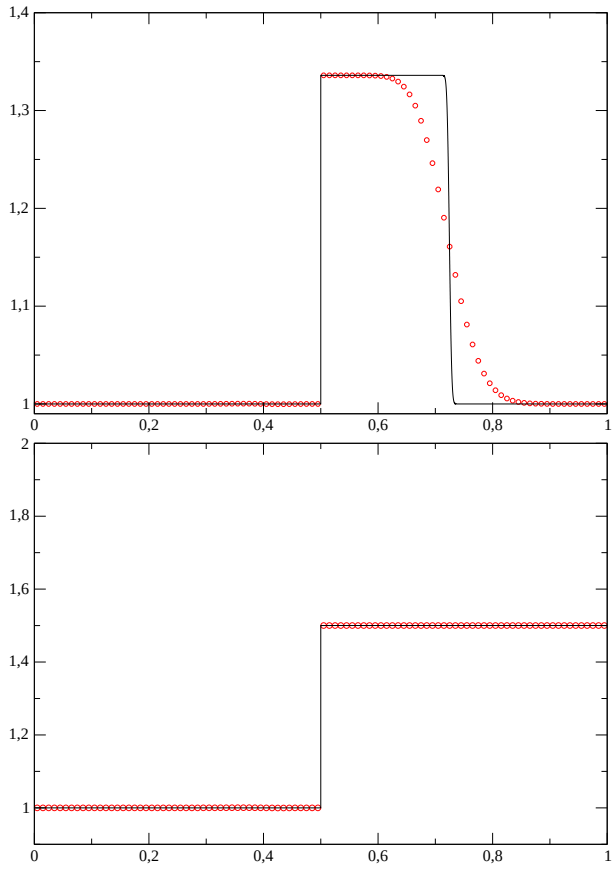

Figure 2: First Riemann problem: density (top) and pressure (bottom) profiles at time $t = 0.6$, using 100 cells -red circles- and 20000 cells -black line-.

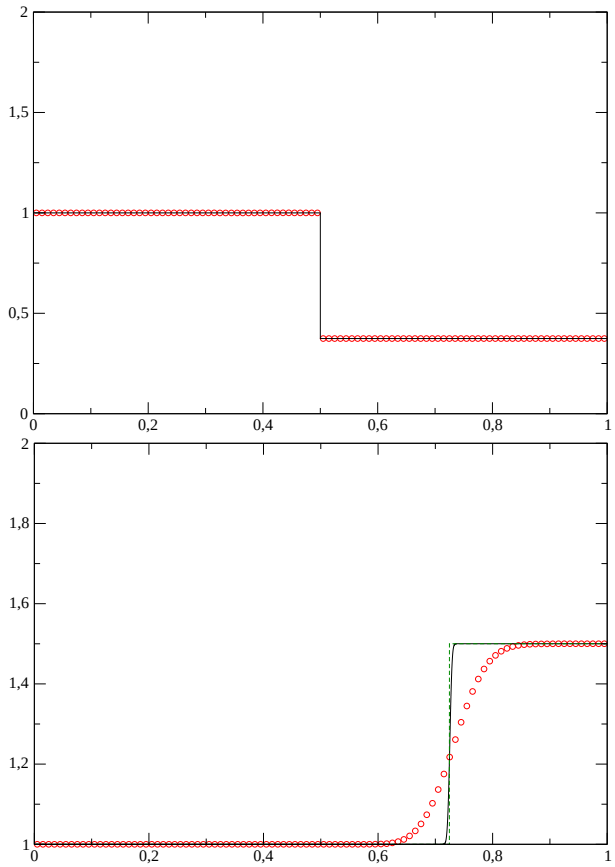

Figure 3: First Riemann problem: velocity (top) and entropy (bottom) profiles at time $t = 0.6$, using 100 cells -red circles- and 20000 cells -black line-, compared with the exact solution -green dashed line-.

5.2.2. Second Riemann problem

We focus now on a test case that has been proposed recently in [21]. The EOS is exactly the same as in the previous case. The solution contains a left-going rarefaction wave, a steady contact discontinuity, a right-going contact discontinuity and eventually a right-going shock wave. The initial data (and the values of the three intermediate states A, B, C separating the four waves) is recalled below:

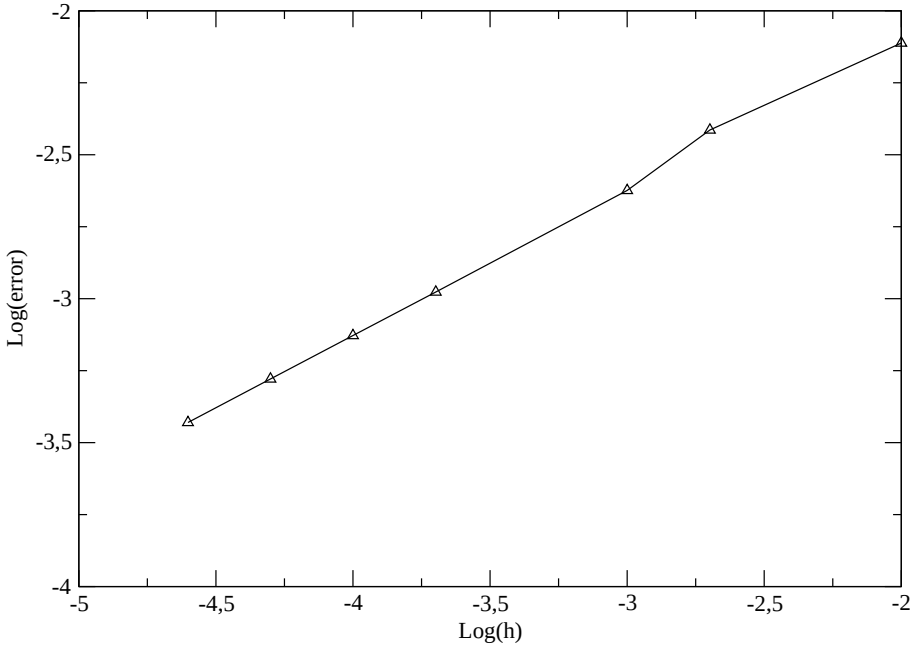

Figure 4: First Riemann problem: L^1 norm of the error for the density at time $t = 0.2243$. The coarser and finer meshes contain 100 and 40000 regular cells respectively, and $h = 1/N$ where N denotes the number of cells.

	Left state	State A	State B	State C	Right state
A	1.	1.	0.4	0.4	0.4
ρ	4.	3.214845	2.540263	2.724432	1.340907
U	0.	80	253.1111	253.1111	25.562711
P	$4. \times 10^5$	29457.78	211839.13	211839.13	75118.155

We recall here that three scalar constraints have been enforced in order to construct this solution, for a given left state, assuming $A_R = 0.4$; these are: $U_A = 80$, $\rho_C/\rho_B = 1.0725$ and $P_R/P_C = 0.3546$ (see [21]).

We compute the solution at time $t = 8.02 \times 10^{-4}$, and we consider rather fine meshes here with 5000 and 20000 regular cells. We first notice that the steady contact discontinuity is perfectly represented, whatever the mesh size is. When focusing on the entropy profiles, no oscillation arises, which slightly differs from what may be noticed beyond the right going shock wave in [21]. The approximate solutions with 5000 cells -red line- and 20000 cells have

been compared with the exact solution on Figures 5, 6.

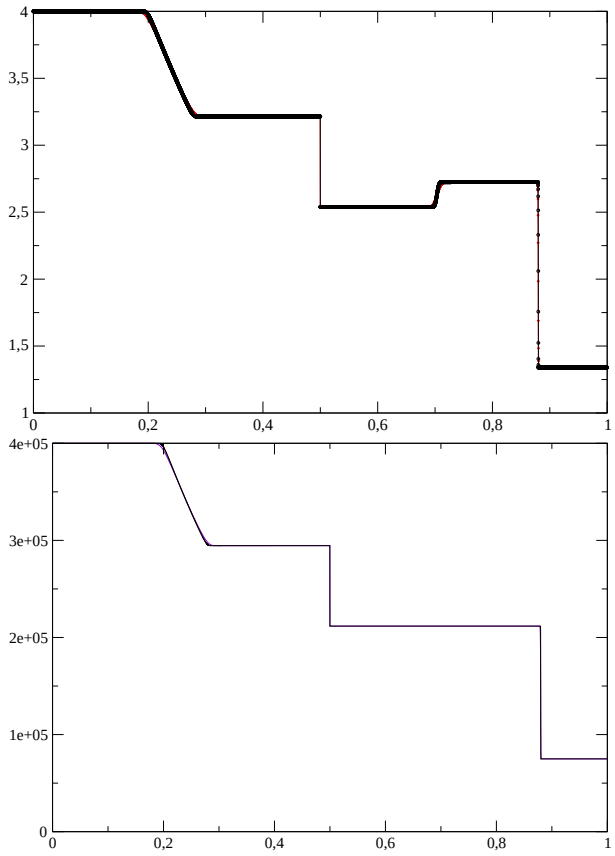

Figure 5: Second Riemann problem: density (top) and pressure (bottom) profiles at time $t = 8.02 \times 10^{-4}$, using 5000 cells -red circles- and 20000 cells -black circles-, compared with the exact solution.

5.2.3. Third Riemann problem

The EOS is still a perfect gas EOS with $\gamma = 7/5$. The computational domain is $[0, 1000]$, and the initial discontinuity is located at $x = 500$. The solution contains a left-going shock wave (whose speed is: $\sigma_1 = -152.26249$), the steady contact discontinuity, a right-going contact discontinuity and also a right-going shock wave ($\sigma_3 = 461.11895$). The initial data (and values of the three intermediate states A, B, C separating the four waves) are the following:

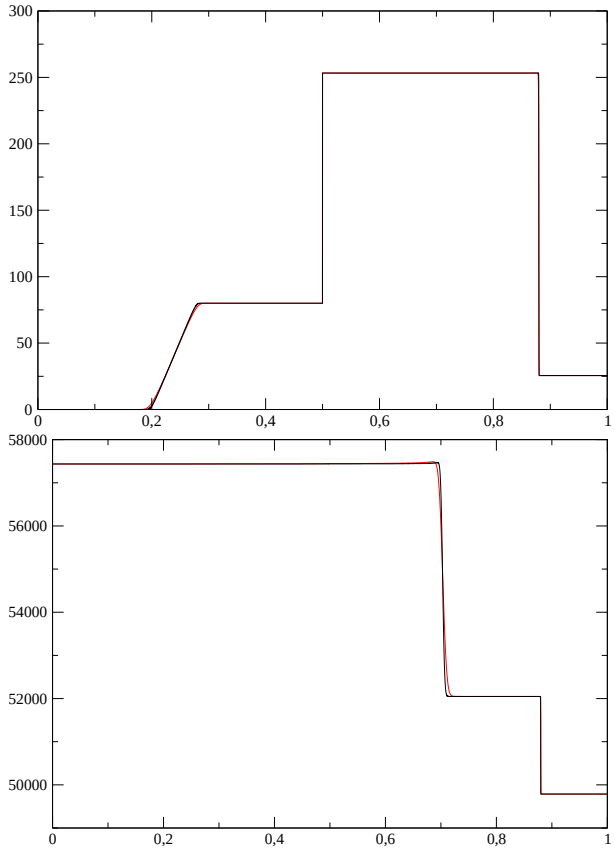

Figure 6: Second Riemann problem: velocity (top) and entropy (bottom) profiles at time $t = 8.02 \times 10^{-4}$, using 5000 cells -red circles- and 20000 cells -black circles-, compared with the exact solution.

	Left state	State A	State B	State C	Right state
A	1.	1.	0.5	0.5	0.5
ρ	0.5	1.	0.842644896	1.	0.5
U	352.26249	100.	237.347904	237.347904	13.5768571
P	36363.6364	$1. \times 10^5$	78686.8994	78686.8994	28613.418

The approximate solutions of density, pressure and velocity are plotted at time $t = 0.8$ on Figures 7 and 8 respectively, considering two distinct meshes with 5000 and 20000 regular cells. Once again, no diffusion arises through the steady contact discontinuity, while the right-going contact discontinuity is smeared (see Figure 7), as it classically happens. The L^1 norm of the

error has been plotted on Figure 9 ; it allows to check that a first order rate of convergence is achieved. This is due to the fact that the steady wave is "perfectly" approximated, and also to the fact that P is a Riemann invariant through the moving contact wave associated with $\lambda_2 = U$.

5.3. Implosion of a bubble

We now consider a difficult test case that simulates the collapse of a spherical bubble of vapour in liquid water that has been generated by a laser beam (see [20]). For that purpose, we assume a perfect invariance under rotation, and thus adopt a pure 1D approach with a variable cross section $A(r) = 4\pi r^2$, for $r \in [0, 1]$. We still assume a perfect gas state law for the fluid (32), setting now $\gamma = 1.01$.

The initial condition is: $W(r < 0.4, t = 0) = W_L$, and $W(r > 0.4, t = 0) = W_R$, where left and right states are given by:

	Left state	Right state
ρ	0.01	1000.
U	0.	0.
P	5	10^5

This test case is difficult since the pressure ratio is very high, and also due to the fact that the cross section tends to 0 when getting close to the left boundary $r = 0$. An entropy correction is of course mandatory due to the strong rarefaction wave that develops during the computation. Otherwise, negative values of pressure and density occur rapidly and the code stops. We use here the efficient parameter-free entropy correction that has been proposed in [14]. The latter correction is only active through one -sonic-interface at each time step.

The flow is somewhat similar to a strong rarefaction wave that propagates over a near-vacuum initial state. We plot on Figures 10, 11, the profiles of the density, pressure, momentum and velocity, focusing on meshes containing 1000, 5000 and 20000 cells respectively, just before the reflexion of the initial left-going shock wave on the left boundary.

Of course all profiles are quite different from what they would be if the cross section were uniform. The results are much sensitive to the mesh refinement at this stage of the computation, owing to the fact that the ratio of

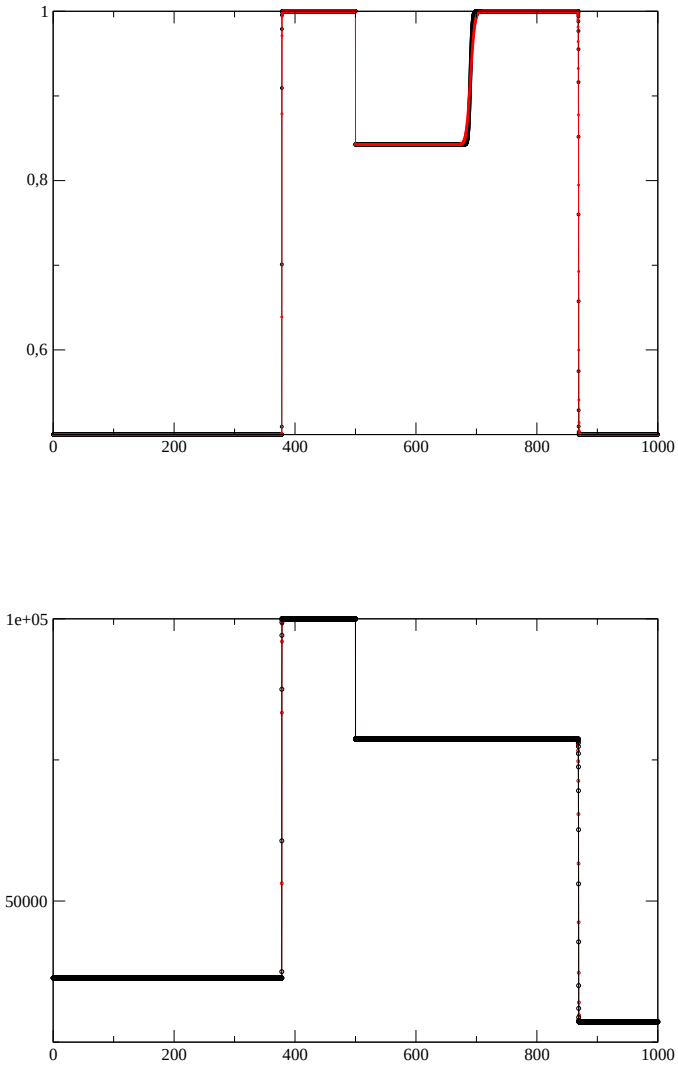

Figure 7: Third Riemann problem: density (top) and pressure (bottom) profiles at time $t = 0.8$, using 5000 cells -red circles- and 20000 cells -black circles-.

cross sections in two neighbouring cells varies much close the left boundary. Figures 12 and 13 show the density-pressure-momentum ditributions at time

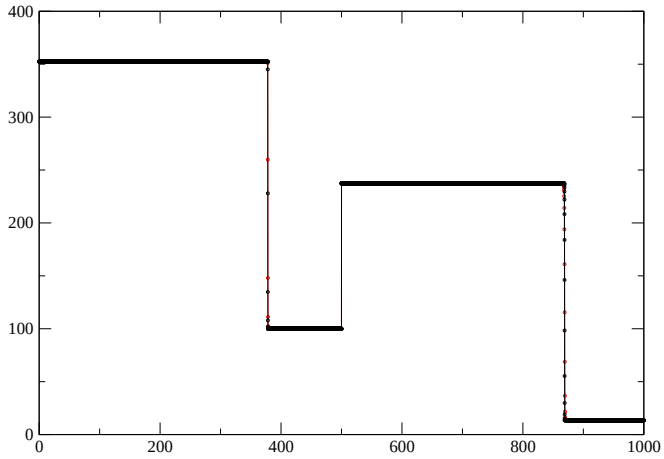

Figure 8: Third Riemann problem: velocity profiles at time $t = 0.8$, using 5000 cells -red circles- and 20000 cells -black circles-.

$t = 0.004$, just before the reflexion of the initial left-going shock wave on the left boundary.

These latter results have been obtained using a mesh with 20000 and 50000 -dotted line- regular cells respectively.

6. Conclusion

The present well-balanced scheme based on VFRoe-ncv interface Riemann solver provides approximations that converge towards correct solutions when discontinuities of the cross section occur in the computation. As already emphasized in [9], the well-balanced property 2 seems mandatory in order to obtain this result. The interface Riemann solver thus requires solving two non-linear scalar equations at each cell interface, which means of course that it is more expensive than the standard VFRoe-ncv scheme (see [8] for instance). However, we underline that the modified well-balanced scheme introduced in [18] and [9] for single and two phase flows respectively, also requires solving two scalar non-linear equations per interface, in order

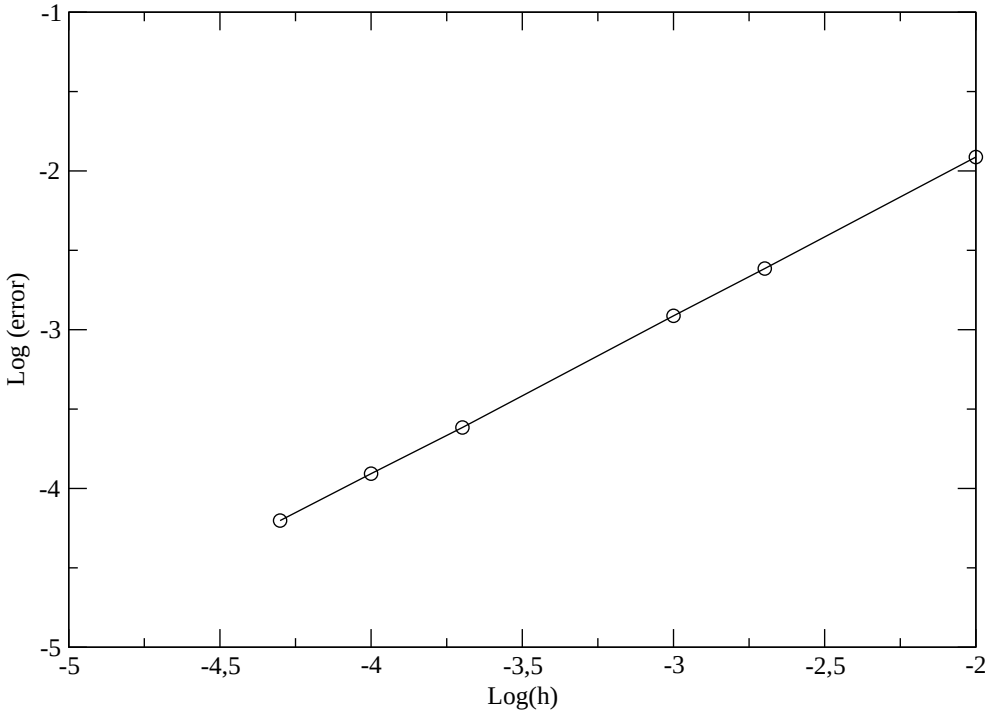

Figure 9: Third Riemann problem: L^1 norm of the error at time $t = 0.8$, focusing on the pressure variable.

to get relevant converged approximations. Hence, the increase of CPU time between WBR and WB-VFRoe-ncv is compensated by the increase of accuracy, for a given mesh size. In practice, the rate of convergence of the scheme WB-VFRoe-ncv is close to $1/2$ in L^1 norm, and thus is almost the same as the one obtained with WBR (see [9]); this result was of course expected, owing to the two contact discontinuities in the governing set of equations.

If we turn to physical considerations, we nonetheless insist that there is

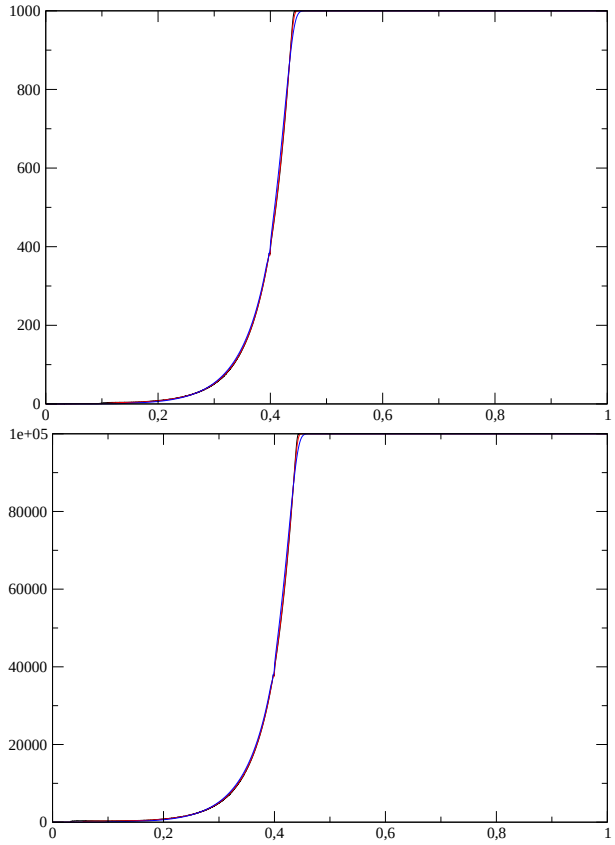

Figure 10: Bubble test case: density (left) and pressure (right) profiles at time $t = 0.004$ using 1000 -blue line-, 5000 -red line- and 20000 -black line- regular cells.

still a need to improve the *formulation of the momentum equation*, so that we may get a better representation of the true flow when a discontinuity occurs in the cross section profile. This has been recently highlighted in [10], and some ideas to cure this point are currently investigated (see [23]).

References

[1] Bouchut F., *"Nonlinear stability of Finite Volume methods for hyperbolic conservation laws, and well-balanced schemes for sources"*, Frontiers in Mathematics series, Birkhauser, 2004.

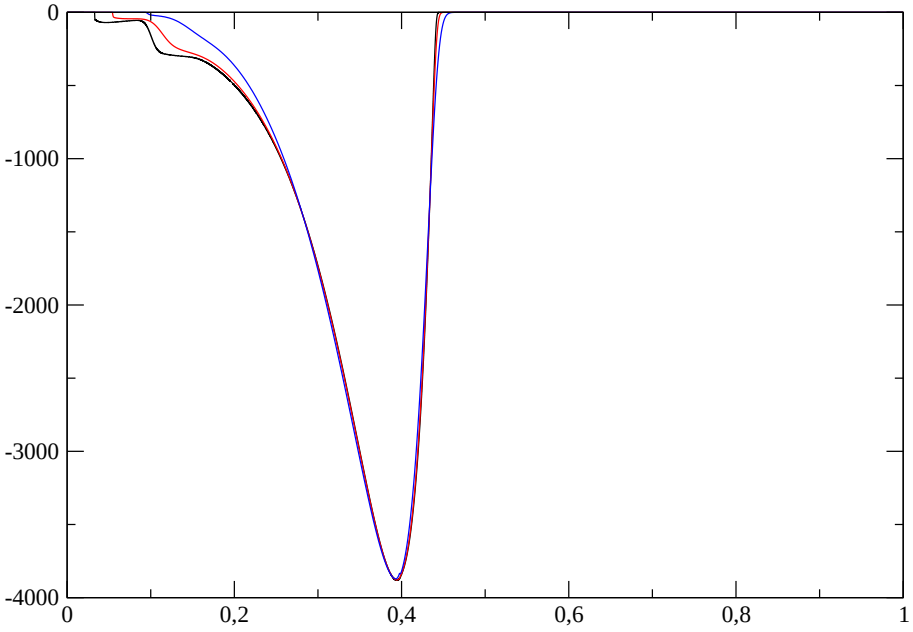

Figure 11: Bubble test case: momentum profiles at time $t = 0.004$ using 1000 -blue line-, 5000 -red line- and 20000 -black line- regular cells.

[2] Bourdarias C., Gerbi S., "A Finite Volume scheme for a model coupling unsteady flows in pipes" *J. Comp. Appl. Math.*, vol. 209(1), pp. 109-131, 2007.

[3] Buffard T., Gallouët T., Hérard J.-M., "A sequel to a rough Godunov scheme. Application to real gases ", *Computers and Fluids*, vol. 29(7) , pp. 813-847, 2000.

[4] Chinnayya A., Le Roux A.Y., Seguin N., "A well-balanced numerical scheme for shallow-water equations with topography: the resonance phenomena", *Int. J. Finite Volumes (electronic)*, http://www.latp.univ-mrs.fr/IJFV/, vol. 1, pp. 1-30, 2004.

[5] Clain S., Rochette D., "First and second-order Finite Volume methods for the one-dimensional non-conservative Euler system ", *J. of Computational Physics*, vol. 228 , pp. 8214-8248, 2009.

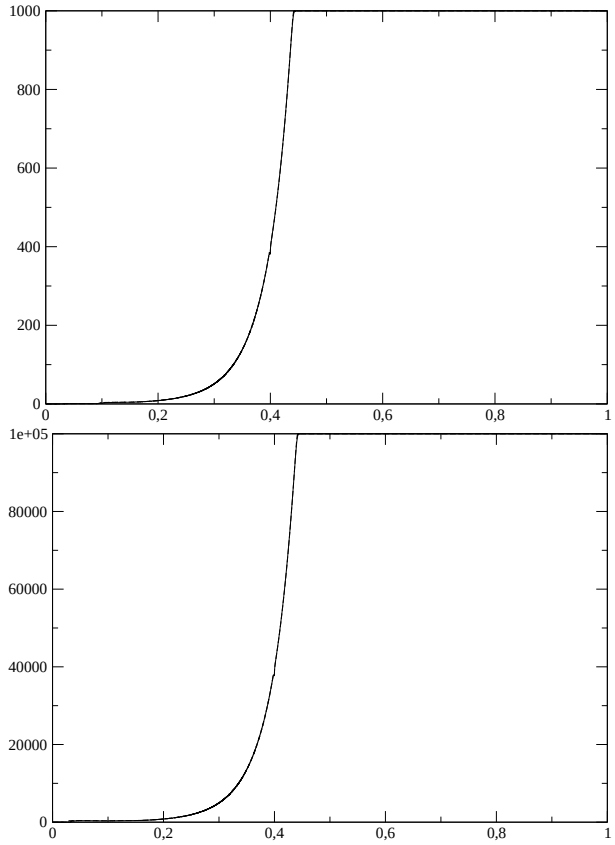

Figure 12: Bubble test case: density (left) and pressure (right) profiles at time $t = 0.004$ using 20000 -plain line- and 50000 -dotted line- regular cells.

[6] Eymard R., Gallouët T., Herbin R., "*Finite Volume methods*", in Handbook of Numerical Analysis, P.G. Ciarlet and J.L. Lions editors, North Holland, vol. VII, pp. 715-1022, 2000.

[7] Gallouët T., Hérard J.-M., Seguin N., "Some recent Finite Volume methods to compute Euler equations using real gas EOS", *Int. J. for Numerical Methods in Fluids*, vol.39 (12), pp. 1073-1138, 2002.

[8] Gallouët T., Hérard J.-M., Seguin N., "Some approximate Godunov schemes to compute shallow water equations with topography", *Computers and Fluids*, vol.32 (3), pp. 479-513, 2003.

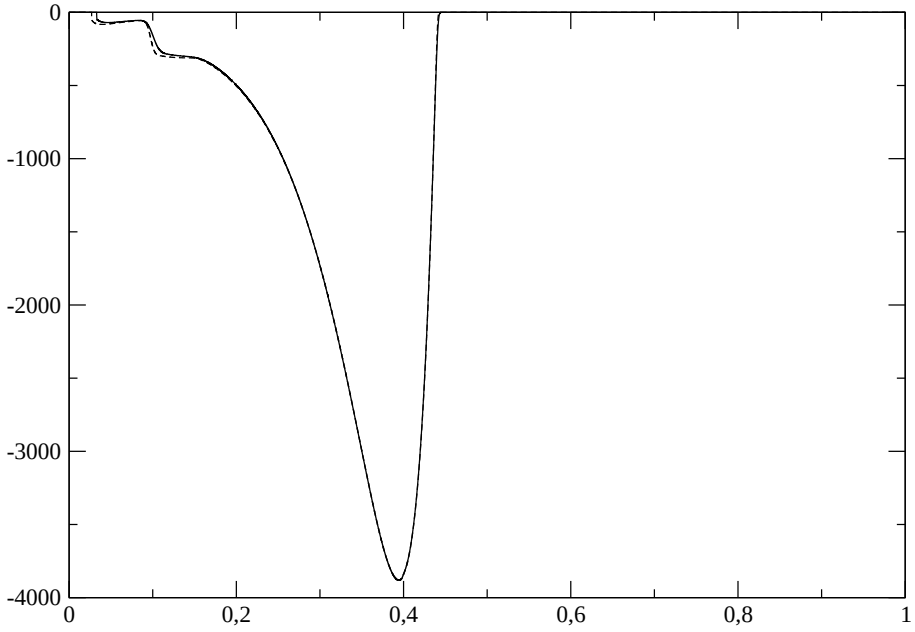

Figure 13: Bubble test case: momentum profile at time $t = 0.004$, using 20000 -plain line- and 50000 -dashed line- regular cells.

[9] Girault L., Hérard J.-M., "A two-fluid hyperbolic model in a porous medium", *Mathematical Modeling and Numerical Analysis*, vol. 44(6), pp. 1319-1348, 2010.

[10] Girault L., Hérard J.-M., " Multidimensional computations of a two-fluid hyperbolic model in a porous medium", *Int. J. Finite Volumes, http://www.latp.univ-mrs.fr/IJFV/*, vol. 7 (1), pp. 1-33, 2010.

[11] Goatin P., Le Floch P., "The Riemann problem for a class of resonant hyperbolic systems of balance laws", *Annales Inst. Henri Poincare*, vol. 21 (6), pp. 881-902, 2004.

[12] Godunov S.K., "Finite difference method for numerical computation of discontinuous solutions of the equations of fluid dynamics", *Mat. Sb.*, vol. 47, pp. 271-300, 1959.

[13] Greenberg J.-M., Leroux A.Y., "A well-balanced scheme for the numerical processing of source terms in hyperbolic equations", *SIAM J. Num. Anal.*, vol. 33 (1), pp. 1–16, 1996.

[14] Helluy P., Hérard J.-M., Mathis H., Müller S., "A simple parameter-free entropy correction for approximate Riemann solvers", *Comptes rendus Mécanique*, vol. 338, pp. 493-498, 2010.

[15] Hérard J.-M., "A rough scheme to couple free and porous media", *Int. J. Finite Volumes (electronic)*, http://www.latp.univ-mrs.fr/IJFV/, vol. 3 (2), pp. 1-28, 2006.

[16] Hérard J.-M., "Un modèle hyperbolique diphasique bi-fluide en milieu poreux", *Comptes rendus Mécanique*, vol. 336, pp. 650-655, 2008.

[17] Kröner D., Le Floch P., Thanh M.-D., "The minimum entropy principle for compressible fluid flows in a nozzle with discontinuous cross section", *Math. Mod. Num. Anal.* , vol. 42(3), pp. 425-443, 2008.

[18] Kröner D., Thanh M.-D., "Numerical solution to compressible flows in a nozzle with variable cross-section", *SIAM J. Numer. Anal.*, vol. 43(2), pp. 796–824, 2006.

[19] Le Floch P., Thanh M.-D., "The Riemann problem for fluid flows in a nozzle with discontinuous cross section", *Commun. Math. Sci.*, vol. 1, pp. 763-797, 2003.

[20] Müller S., Bachmann M., Kroninger D., Kurz T., Helluy P., " Comparison and validation of compressible flow simulations of laser-induced cavitation bubbles", *Computers and Fluids*, vol. 38, pp. 1850-1862, 2009.

[21] Rochette D., Clain S., "Two-dimensional computation of gas flow in a porous bed characterized by a porosity jump", *J. of Computational Physics*, vol. 219, pp. 104-119, 2006.

[22] Rochette D., Clain S., Buffard T., "Numerical scheme to compute a compressible flow in variable porosity media", *Int. J. of Computational Fluid Dynamics*, vol. 19(4), pp. 299-309, 2005.

[23] Saleh K., *P*hD thesis, in preparation, Université Pierre et Marie Curie, Paris, France.

[24] Thanh M.-D., "The Riemann problem for a non-isentropic fluid in a nozzle with discontinuous cross-sectional area", *SIAM J. Appl. Math.*, vol. 69(6), pp. 1501–1519, 2009.

7. Answers and comments

- Typos have been corrected.
- There are now two distinct Riemann problems involving the four waves (see sections 5.2.2 and 5.2.3 in the section devoted to numerical results). We think that these, which involve shocks and rarefaction waves, are rather convincing. In particular, we retrieve the expected rates of convergence (first order for velocity and pressure, and 1/2 for the density), for fine enough meshes. This confirms that the steady contact wave is very well approximated (otherwise the rate would be lower for both U and P).
- We thank the reviewer who pointed out to us reference [24] (now included in this second revision), and also for his useful comments.